Investigation of the transition of amorphous Ti-thiolate prepared by hybrid atomic layer deposition/molecular layer deposition into titanium disulfide ultrathin film

Petros Abi Younes, Ashok-Kumar Yadav, Medet Zhukush, Van-Hoan Le, Hervé Roussel, Marie-Ingrid Richard, Clément Camp, Kai Szeto, Gianluca Ciatto, Nathanaelle Schneider, et al.

Investigation Of The Transition Of Amorphous Ti-thiolate prepared by Hybrid Atomic Layer Deposition/Molecular Layer Deposition Into Titanium Disulphide Ultra-Thin Film

Petros Abi Younes,[1,2] Ashok-Kumar Yadav,[3] Medet Zhukush,[4] Van-Hoan Le,[2] Hervé Roussel,[1] Marie-Ingrid Richard,[5,6] Clément Camp,[7] Kai Szeto,[7] Gianluca Ciatto,[3] Nathanaelle Schneider,[8] Elsje Alessandra Quadrelli,[4] Nicolas Gauthier,[2] and Hubert Renevier[1]

[1)] *Univ. Grenoble Alpes, CNRS, Grenoble-INP, LMGP, Grenoble, France*

[2)] *Univ. Grenoble Alpes, CEA, LETI, F-38000 Grenoble, France.*

[3)] *Synchrotron SOLEIL, Beamline SIRIUS, L'Orme des Merisiers, Saint-Aubin, F-91192, Gif sur Yvette, France.*

[4)] *Université de Lyon, IRCELYON, Institut de Recherche sur la catalyse et l'environnement (UMR 5256 CNRS Université Lyon1), 2 av. Albert EINSTEIN, 69100 Villeurbanne, France.*

[5)] *Univ. Grenoble Alpes, CEA Grenoble, IRIG, MEM, NRS, 17 rue des Martyrs 38000 Grenoble, France.*

[6)] *European Synchrotron Radiation Facility, 71 Avenue des Martyrs, 38043 Grenoble, France*

[7)] *Université de Lyon, CP2M, Laboratory of Catalysis, Polymerization, Processes and Materials, UMR 5128 CNRS-UCB Lyon 1-CPE Lyon, Institut de Chimie de Lyon, 69616 Villeurbanne, France.*

[8)] *IPVF (UMR 9006), Institut Photovoltaïque d'Ile-de-France, 18 boulevard Thomas Gobert, 91120 Palaiseau, France.*

(Dated: 22 February 2023)

Amorphous organic-inorganic hybrid thin films (Ti-thiolate) deposited on thermal SiO_2 substrate by Atomic Layer Deposition/Molecular Layer Deposition (ALD/MLD) are converted into textured titanium disulphide (TiS_2) ultra-thin films, of thickness down to 5.5 nm, upon annealing under $Ar/H_2(5\%)$ atmosphere at mild temperature (300 °C). Two annealing strategies were investigated by *in situ* synchrotron X-ray fluorescence, allowing us to master the mineralization of the amorphous Ti-thiolate into titanium disulphide. Stoichiometry and crystallinity of the thin films were characterized by X-ray photoelectron spectroscopies, Raman scattering and X-ray absorption at the S K-edge. Lamellar structure parallel to the substrate surface was observed by transmission electron microscopy.

I. INTRODUCTION

Transition metal dichalcogenides (TMDCs) have attracted great interest due to their ultimate level of miniaturization. The interest of using TMDCs is related to its lamellar structure which permits to reduce the layer stack to few layers or even to a monolayer, thanks to weak van der Waals bonds between the layers. A TMDC layer with the chemical formula MX_2 consists in the superposition of a plane of transition metal atoms (M=Ti, Mo, W, Nb,...) sandwiched in between two planes of chalcogen atoms (X=S, Se and Te), with M-X covalent bonds. TMDCs exhibit thickness-dependent physical properties, which is considered an interesting feature since its variation permits to cover a wide range of potential applications.[1–3]

Lamellar titanium disulphide TiS_2, based on S-Ti-S stacked layers separated by van der Waals gaps, is considered to be integrated in emerging devices for various applications. Indeed, TiS_2 can be used in new supercapacitor electrodes for rechargeable batteries[4,5], or for new hybrid based material grown with organic intercalation[6,7]. TiS_2 also covers additional applications including thermoelectric[5,8], optics[4], hydrogen storage[9] and photovoltaic in TiS_2/TiO_2 heterostructures.[10]

The deposition of TiS_2 ultra-thin films is getting more attention, since ultra-thin films showed a potential employment in high-energy density reversible lithium batteries.[11] In addition, the number of TiS_2 layers along with its stoichiometry, define its semimetal or semiconductor nature.[12] All the elements mentioned above emphasize the need of TiS_2 thin films. However, finding the suitable large-scale growth technique is challenging.

Among the growth methods, the mechanical exfoliation method of TiS_2 bulk crystals is not suitable for large-scale production, since it cannot produce high-quality uniform films. Alternative strategies have been reported, such as Physical Vapor Deposition (PVD), Chemical Vapor Deposition (CVD) methods, or chalcogenization of metal oxides.[13,14] TiS_2 was synthesized by different growth techniques such as CVD[15–20], chemical exfoliation method[21], wet chemical synthesis[22], and to a limited extent, by ALD.[1,5,23–29] The properties of the grown material appear to be highly dependent on the substrate nature whereas no high quality ultra-thin films could be obtained.[1,5,23–25]

Atomic Layer Deposition (ALD) is an ideal growth technique to produce a conformal film with precise thickness level control. This gas-phase growth technique based on sequential, self-limiting surface reactions, ensures good reproducibility

and homogeneity over the substrate area.[30] In the case of layered TMDCs, ALD growth of ultra-thin films faces specific difficulties: the control of the nucleation and 2D growth of one or a few crystalline and textured MX_2 layers on non epitaxial substrate is definitely not straightforward. As the basal planes of the crystalline MX_2 layer are chemically inert, -SH moieties are present at structural defects and edges where further chemical reactions with the metal precursor molecules will occur.[31,32] This leads to discontinuous poorly textured and crystalline thin films. If possible and relevant, this effect can be mitigated by depositing on a well-chosen crystalline and oriented substrate surface that promotes 2D growth.[33–36]

A different approach, which is used herein, aims to avoid the co-occurence of growth and crystallization, and can be applied to amorphous substrates. The use of an organic precursor (co-reactant) during a so-called Atomic Layer Deposition/Molecular Layer Deposition (ALD/MLD) process performed at relatively low temperature, generates an amorphous inorganic-organic hybrid thin film.[37,38] The transition from amorphous to crystalline material requires a subsequent thermal annealing treatment, during which the loss of most of the organic moieties permits the crystallization to occur.[39]

This approach (ALD/MLD and post-annealing) has been recently used by our team to grow TiS_2 ultra-thin films.[40] First, amorphous film (Ti-thiolate) were generated by ALD/MLD at low temperature (T_{sub}= 50 °C) by alternating tetrakis dimethylamido titanium ($Ti(NMe_2)_4$, TDMAT) and 1,2-ethandithiol (EDT) pulses on a non- epitaxial substrate (thermal silicon oxide substrate, widely used in microelectronics). Secondly, the Ti-thiolate thin film was annealed under Ar/H_2(4%) at 450 °C for 30 min leading to continuous, smooth, homogeneous films. Hard X-ray Photoelectron Spectroscopy (HAXPES) showed that the annealed deposited film is composed of near stoichiometric layers of TiS_2. Transmission Electron Microscopy (TEM) showed TiS_2 layers that tend to be almost parallel to the substrate surface. Besides, the obtained TiS_2 thin films showed a semi-conductor behavior.[40] However, the presence of C-containing organic fragments and bridging sulfide $(Sn)^2$ pairs indicates a non-complete annealing. Also, sulfur loss occurring during the annealing step makes it difficult for obtaining ultra-thin films ($\leq$ 10nm) of TiS_2. Therefore, finding the adequate thermal annealing conditions to reach ultra-thin TiS_2 films is of primary importance.

This work aims at understanding the transition from amorphous Ti-thiolate into crystalline TiS_2. Two different thermal annealing strategies capable of producing stoichiometric ultra-thin layers of TiS_2 were determined. The necessity of using different annealing strategies depending on the Ti-thiolate thickness and sulfur content is demonstrated and discussed herein. *In situ* monitoring by X-ray fluorescence (XRF) is used to track the S/Ti ratio during the annealing. Additional *ex situ* characterization such as X-ray Photoelectron Spectroscopies, elemental and structural analysis (TEM and Raman spectroscopy) were performed on the annealed TiS_2 layers to characterize crystallinity, structure, and stoichiometry. Overall, this study has allowed the in-plane crystallization of ultra-thin lamellar stoichiometric TiS_2 at annealing temperature as mild as 300 °C.

II. EXPERIMENTAL SECTION

A. Thin film fabrication

ALD/MLD growth of the hybrid organic-inorganic Ti-thiolate was performed on 100 nm thick thermal amorphous SiO_2 on Si wafer substrates, at substrate temperature T_{sub} = 50°C from tetrakis-dimethylamido titanium (TDMAT) and 1,2-ethanedithiol (EDT), as reported previously.[40] Thiolate films were grown with 20, 40 and 60 ALD/MLD cycles.

Annealing treatments were carried out under 100 standard cubic centimeter per minute (sccm) flow of Ar/H_2(5%), with a temperature ramp equal to 10 °C/min. Annealing temperature profiles were set depending on the annealing strategy and are described in part III. The reference TiS_2 powder sample was purchased from $Merck^{TM}$ (CAS number: [12039-13-3]).

B. Thin film *in situ* characterization

The two-step process, i.e. ALD/MLD growth followed by thermal annealing, was developed in a custom-built portable reactor designed to be installed onto the 6-axis tower of the $Newport^{TM}$ diffractometer of beamline SIRIUS[41] of SOLEIL synchrotron facility. The set-up allows to use a complementary suite of *in situ* synchrotron x-ray techniques (reflectivity, grazing-incidence fluorescence, diffraction, and absorption).[42]

Synchrotron radiation XRF and XRR were performed *in situ* during both steps, using similar optical elements and beam setup (energy, intensity, incident angle) than reported previously.[40]

In situ X-ray Absorption Near-Edge structure Spectroscopy (XANES) was performed at the S K-edge in fluorescence detection mode using same optical elements and measurement parameters (energy scanning mode, monochromator and undulator movements; mirrors, geometry) as described previously.[40]

C. Thin film *ex situ* characterization

The XPS (X-ray Photoelectron Spectroscopy) and HAXPES (Hard X-ray Photoelectron Spectroscopy) data were measured using a PHI Quantes at the Nanocharacterization Platform (PFNC) with two different monochromatized sources, Al K_α (hν=1486.6 eV) and Chromium K_α (hν = 5414.7 eV). The analysis depth using Cr K_α source is about three times deeper than with the Al K_α source.[40] Benefiting from a larger sampling depth opens opportunities to minimize the contribution of the upper surface of the sample, possibly altered by the atmosphere, in the overall spectra. Samples were prepared using a metallic clamp to ensure the electrical contact with the sample holder. Measurements using Cr source have been done at a fixed angle of θ=45° and for the Al one at different angles using Angle-Resolved XPS (or ARXPS) (θ=15°, 45°, and 90°), where θ is the angle between the surface and the analyzer. Using the formula d=3 λ sinθ (where λ is the

photoelectron mean free path using TPP2M equation[43]), the analysis depth were calculated to 2.3, 4.9, and 6.8 nm, respectively in the case of ARXPS and to 15.7 nm with the HAXPES. Data treatment were carried out with the CasaXPS software. We used the relative sensitivity factors (RSF) provided by the instrument to perform the quantification of the elements with Al source whereas theoretical RSF were used to quantify the stoichiometry of the obtained TiS_2 layers with Cr source.[44] For spectral calibration, C 1s core peak from adventitious carbon was considered with a binding energy of 284.8 eV.[27] A non-linear Shirley-type background was processed for peak fitting and the deconvolution of the peaks was obtained using 30% Lorentzian and 70% Gaussian line shapes.[2] For the surface oxide thickness calculation, we used the Ultra Thin Film Analysis of Multipak software developed by Physical Electronics (https://www.phi.com/surface-analysis-equipment/system- software.html).

Post-growth annealed samples have been characterized by Raman Spectroscopy using a Renishaw In-Via spectrometer, equipped with a Peltier cooled (CCD) detector and 1800 groove.mm^{-1} grating. Raman spectra were recorded in the backscattering geometry. A 532 nm laser diode was used an excitation source with a typical laser power of 0.07 mW. The light was focused onto the sample surface by a 100 x (0.85 numerical aperture) short working objective. The resulting spot diameter was around 0.7 μm. The acquisition time of each spectrum was 30s and the number of accumulations was equal to 5. Raman spectrum were analysed using the *LabSpec*5^{TM} software (HORIBA). Raman spectra were normalized to the intensity of the A1g mode and fitted with Lorentzian function for A1g mode, and with a Gaussian-Lorentzian function (GL(30%)) for the Eg and Sh modes.

Transmission electron microscopy (TEM) observations were carried out at 200 kV with a Tecnai Osiris TEM (Thermo Fisher Scientific) and equipped with a high brightness X-FEG gun and a Super-X Energy Dispersive x-ray (EDX) system comprising four detectors; Note that the analyzed sample was coated with a carbon protective layer.

XANES at the S K-edge were also carried out after transferring the samples inside SIRIUS High Vacuum (HV) diffractometer by means of a glove box.[45] XANES spectra were recorded by scanning the incoming energy step-by-step and measuring the sample fluorescence with the four-element Silicon Drift Detector (SDD). The beamline optics setup was the same as described above for the *in situ* XANES at the S K-edge.

D. Study on silica beads

ALD/MLD experiments were performed on silica powder (AEROSIL® 200 fumed silica; 15-20 nm particles; 200 m^2/g surface area (BET method)) previously dehydroxylated at 700°C, as reported in our previous work.[40] Thiolate films were grown with 2 ALD/MLD cycles of TDMAT and EDT following the procedure described elsewhere.[40] Annealing treatments of the ensuing thiolate were carried out in an integrated system enabling *in situ* DRIFT coupled GC-MS analysis of the gaseous by-products (See supplementary material at [URL will be inserted by AIP Publishing] for Figure S1)

III. RESULTS AND DISCUSSION

The synthesis proceeds with the growth of an amorphous Ti-thiolate at substrate temperature T_{sub}=50°C, followed by annealing. To gain insights into the transition from amorphous to crystalline and control it, *in situ* experiments using the synchrotron X-ray radiation were performed and combined with *ex situ* characterization (XPS/HAXPES). The evolution of the [S]/[Ti] ratio during both steps was insightful to explore two new annealing strategies.

A. *In situ* monitoring of thiolate ALD/MLD growth by x-ray Fluorescence (XRF)

To quantify the amounts of Ti and S deposited on the surface of the sample, *in situ* analyses were obtained by monitoring the Ti and S by XRF during each ALD/MLD cycle.[40] Note that *in situ* measurements are necessary as the Ti-thiolate is not stable in ambient conditions. The evolution of Ti and S K_α fluorescence intensity as a function of ALD/MLD cycle number during the growth of a 60-cycle ALD/MLD Ti thiolate was recorded (See supplementary material at [URL will be inserted by AIP Publishing] for Figure S2).

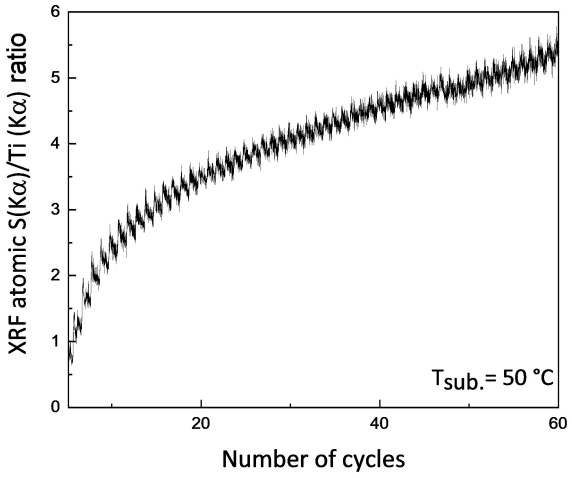

FIG. 1. XRF [S]/[Ti] ratio (calibrated from XPS/HAXPES data of a reference stoichiometric TiS_2 sample) during the growth of a 60 ALD/MLD cycles Ti-thiolate.

The existence of a transient regime at the early stage of the process is due to the interaction of the thermally grown 100 nm SiO_2 substrate active surface with the first precursor pulses. Beyond, a steady XRF intensity increase of both XRF signals could be observed.

Figure 1 shows the evolution of the calibrated XRF [S]/[Ti] ratio. The raw XRF intensity ratio S/Ti was calibrated with the total XRF [S]/[Ti] ratio of a stoichiometric reference sample. The reference sample was prepared from 80 ALD/MLD cycles and annealed under $Ar/H_2(4\%)$ at 450 °C for 30 min; its total thickness obtained by XRR was equal to 30 nm. For such thickness, the contribution of the oxidized regions present on the top of the TiS_2 and at the SiO_2/TiS_2 interface, is small. Indeed, XPS/HAXPES data confirmed that the S/Ti ratio, corresponding to the S bound to Ti, was very close to 2 (2.1), as expected for TiS_2 layers. One observes that [S]/[Ti] XRF intensity ratio does not stay constant and range from 0.8 (early stage) to 5.5 (higher cycle number). After 60 ALD/MLD cycles, the Ti-thiolate thickness was found to be 42±3 nm from the XRR curve fit measured *in situ*.

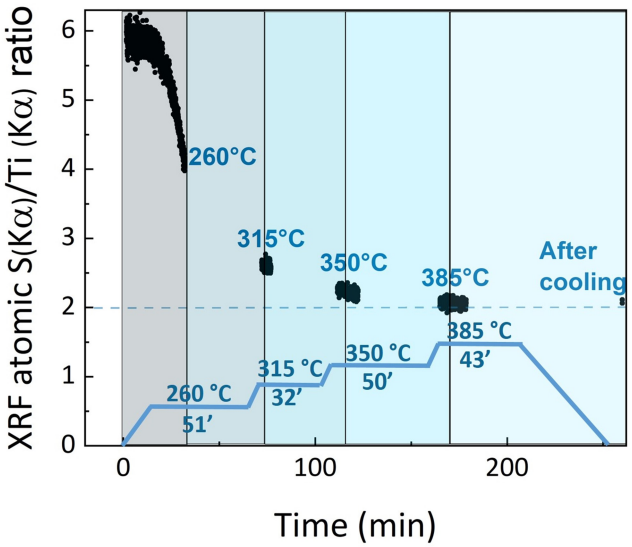

FIG. 2. Calibrated XRF [S]/[Ti] atomic ratio as a function of time and substrate temperature, during the annealing under $Ar/H_2(5\%)$ of a 60-cycle ALD/MLD Ti-thiolate. This annealing is referred as strategy A.

B. Thermal annealing strategies

$Ar/H_2(5\%)$ was selected as annealing gas because of the capability of H_2 to facilitate sulfur extrusion from sulfur-rich TiS_{2+x} compounds[46] (for instance, less S-S pairs were detected in the case of $Ar/H_2(5\%)$ comparing to N_2). The temperature ramp value was 10°C/min, as it prevents major sulfur loss during annealing or in other words, the formation of sub-stoichiometric layer.[47,48] Two annealing strategies, herein noted A and B, were optimized by tracking the evolution of the XRF [S]/[Ti] atomic ratio aiming to produce ultra-thin stoichiometric TiS_2 films. Strategy A consists in increasing the temperature by steps while monitoring the XRF [S]/[Ti] ratio. Strategy B is a unique low temperature plateau, deduced from strategy A.

1. Thermal annealing strategy A

a. Strategy description

The as-grown Ti-thiolate sample was annealed *in situ* under $Ar/H_2(5\%)$ flow, starting from thiolate substrate temperature (T_{sub}=50 °C). Figure 2 shows the evolution of the calibrated XRF [S]/[Ti] ratio along with the annealing temperature profile. The temperature plateau were decided live by checking the rate of decay of the [S]/[Ti] atomic ratio. The temperature plateau duration corresponds to the time necessary for the acquisition of Extended X-Ray Absorption Fine Structure (EXAFS) spectra (not presented in this publication) explaining the absence of experimental points in these regions.

From T_{sub} = 50 °C to 260 °C a large decrease of the [S]/[Ti] ratio was observed ([S]/[Ti]= 5.8 to 4.0). It keeps decreasing from T_{sub} = 260 °C to 315 °C ([S]/[Ti] = 4.0 to 2.6) to reach at T_{sub} = 350°C a [S]/[Ti] ratio slightly above 2. To quickly achieve a stoichiometric sample, the annealing temperature was risen up to 385 °C. Finally, after cooling down to room temperature, the [S]/[Ti] ratio remained very close to 2.

When applying this annealing strategy, an important behavior was noticed, i.e. a major decrease of the ratio before reaching 315 °C, by about a factor of 2. This can be explained by two main reasons. A first one is likely related to the annealing atmosphere ($Ar/H_2(5\%)$), since H_2 is known to improve the sulfur extrusion from sulfur-rich TiS_{2+x} phases.[46]

The second one is provided by chemical experimental modeling carried on high surface area silica beads 3D substrate, herein called silica nanobeads.[40,49] Figure 3 shows the *in situ* Diffuse Reflectance Infrared Fourier Transform (DRIFT) spectra of silica powder nanobeads acquired during the annealing treatment ($T_{annealing}$ = 20 °C to 500 °C) of a 2-cycle ALD/MLD Ti-thiolate. The evolution of IR absorbance of the solid over temperature (see Figure 3) showed mineralization of the solid, which is the intensity decrease of all bands associated with thiolate organic fragments starting below 100 °C leading to a fully inorganic sample by 300 °C. Indeed, signals at around 2700-3000 cm^{-1}, assigned to organic moieties CH_x stretching vibration modes, are almost completely disappeared at 300 °C, confirming that the loss of organic moieties occurs below 300 °C. Over the annealing procedure, the IR component centered at 3650 cm^{-1} assigned to the vibration mode of surface hydroxyl groups, substantially increases. This datum is coherent with the fact that annealing induces densification of the phase (as expected for the thiolate to sulfide transition). As shown elsewhere, the starting amorphous thiolate achieves maximum chemical coverage.[40] The densification of such a thiolate to sulfide can thus lead to discontinuous layers and hence hydroxyl regeneration. Concomitant analysis of the gas phase (see supplementary material at [URL will be inserted by AIP Publishing] for Figure S3) showed the release of various gaseous fragments such as H_2S, ethylene, hydrogen disulfide, methylisocyanide, thiirane, and ethanethiol. Possible mechanistic pathways for the mineralization of the surface sites to titanium disulfide and sulfide, and fragmentation of some part of the ligands to ethylene,

H_2S, thiirane, methylisocyanide are also presented (see supplementary material at [URL will be inserted by AIP Publishing] for Figure S4). In summary, the obtained results on silica nanobeads corroborated the datum acquired on silicon wafer where the major decay of the [S]/[Ti] ratio is observed from 50 °C to 315 °C, and provide possible mechanistic pathways.

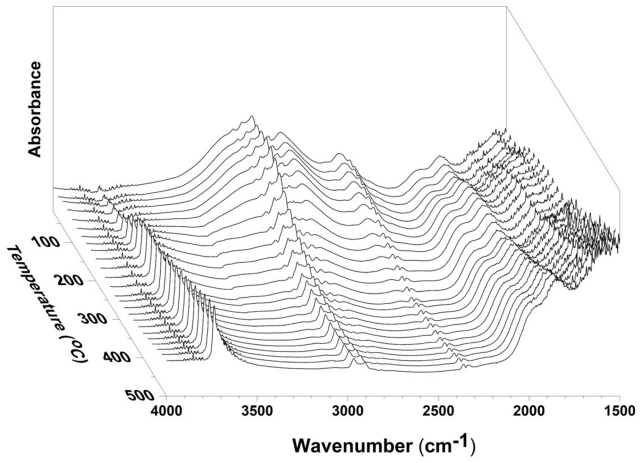

FIG. 3. *In situ* infrared spectra of the silica nanobeads-supported Ti thiolate obtained by 2 ALD/MLD cycles recorded upon thermal treatment from 20 °C to 500 °C

The annealing strategy A gives insights on the process to apply en route to stoichiometric TiS_2 layers. Nevertheless, additional analyses were required to validate its efficiency. Hence, elemental and structural analyses were performed on the annealed TiS_2 films to characterize their stoichiometry, crystallinity and structure.

b. TiS_2 layer chemical composition: Photoelectron Spectroscopy analyses

In order to confirm the atomic ratio determined *in situ* by XRF (Figure 2) and obtain further information on chemical bonding, ARXPS experiments were carried out on the annealed 60-cycle ALD/MLD films. Figure 4 shows the XPS spectra of Ti 2p, S 2p, and C 1s core peaks. TiS_2 is known to convert to TiO_x by exposure to air.[50] For this reason the Ti 2p XPS spectra (Figure 4 (a-d-g)) present two different Ti 2p3/2:2p1/2 spin-orbit doublets. The most intense at high binding energy (458.8 eV and 464.5 eV) corresponds to titanium oxysulfide (TiO_xS_y).[51–54] The less intense doublet (457.0 eV and 462.7 eV) is assigned to TiS_2.[53–55]. The TiS_2 contribution significantly increases as the depth analysis increase, confirming that the oxide is mainly located at the topmost surface of the deposited film. Assuming that the oxidized top layer TiO_x is homogeneous, non-porous, and covering the TiS_2 film with an average composition, a simple model allows to estimate its thickness at around 2nm.[56]

The S-2p XPS spectra shown in Figure 4 (b-e-h) present also two S 2p3/2 :2p1/2 components. The intense doublet (161.2 eV and 162.3 eV, spinorbit doublet of S2p species) corresponds to TiS_2.[51,54] The weak doublet signal (162.8 eV and 164.0 eV) could be attributed to different species such as a S-S pair and/or to C-S bonds. Based on the widening of this weak peak component, we could also assign this environment, to a combination of $(S_n)^{2-}$ bridging sulphur (where n=2,4).[57] In addition, it could be referred to titanium oxysulfide environment in connection with the oxidized part already detected on the surface of the TiS_2 film.[27,52,58,59] ARXPS data shows a large amount of carbon inside the thin films (see Figure 4 (c-f-i)) and not only at the top surface of the layer. Indeed, the C 1s core level spectra exhibit three components originating from different sources, which do not decrease with the thickness analysis. The main, which corresponds to C-H/C-C bonding, could originate from adventitious carbon but also from the incomplete reaction of TDMAT.[24] Note that the presence of graphitic carbon is not to be excluded, as observed in MoS_2 and WS_2 thin films obtained by similar methods.[49] In addition, the C1s core spectrum shows the presence of oxidized carbons (C-O and C=O) coming from surface contamination[27] (peaks at 286.2 and 288.8 eV respectively). Importantly, the component at 286.6 eV could also be assigned to C-S bonds indicating an incomplete reaction of EDT.

Binding energies (BE) and atomic concentrations (at.%) of the different chemical environments identified by XPS are reported for better clarity (see supplementary material at [URL will be inserted by AIP Publishing] for Table S1). The quantitative results permit to calculate the atomic ratio of [S]/[Ti] considering the Ti2p and S2p doublets attributed to TiS_2. It is equal to 1.9, confirming that the deposited film is composed of quasi-stoichiometric TiS_2.

The small depth analysis of XPS remains a major limiting factor to study buried interfaces, since the obtained TiS_2 thin films are oxidized in ambient conditions. For this reason, HAXPES measurements were conducted to investigate the in-depth chemical composition of the TiS_2 film. Both Ti2p and S2p spectra are presented in Figure 5. Binding energies (BE) and atomic concentrations (at.%) of the different chemical environments identified by HAXPES are also reported (see supplementary material at [URL will be inserted by AIP Publishing] for Table S2). The doublets position and attribution are the same as those previously discussed in the ARXPS study. Noticeably, the most intense doublet in Figure 5-a is assigned to TiS_2; thus HAXPES measurements limits the contribution of oxidized layer at the surface of the TiS_2 and leads to an accurate deconvolution of the titanium spectra. Concerning the S-2p XPS spectrum presented in Figure 5-b, the amount of bridging sulphur and sulphur residues from EDT characterized by components at higher binding energy does not decrease meaning that the mentioned sulfur species are located throughout the thickness of the film. Similarly, the carbon content is not assigned only to surface contamination. With chromium source, the atomic ratio of [S]/[Ti] obtained is equal to 2.3. Since the obtained value is actually the same for a reference crystalline stoichiometric TiS_2 powder, this indicates that the deposited film of TiS_2 is close to the stoichiometric one.

Both XPS and HAXPES confirm that the annealing strategy A, under $Ar/H_2(5\%)$ applied on 60-cycle ALD/MLD thiolate, is efficient to generate a film composed of quasi-

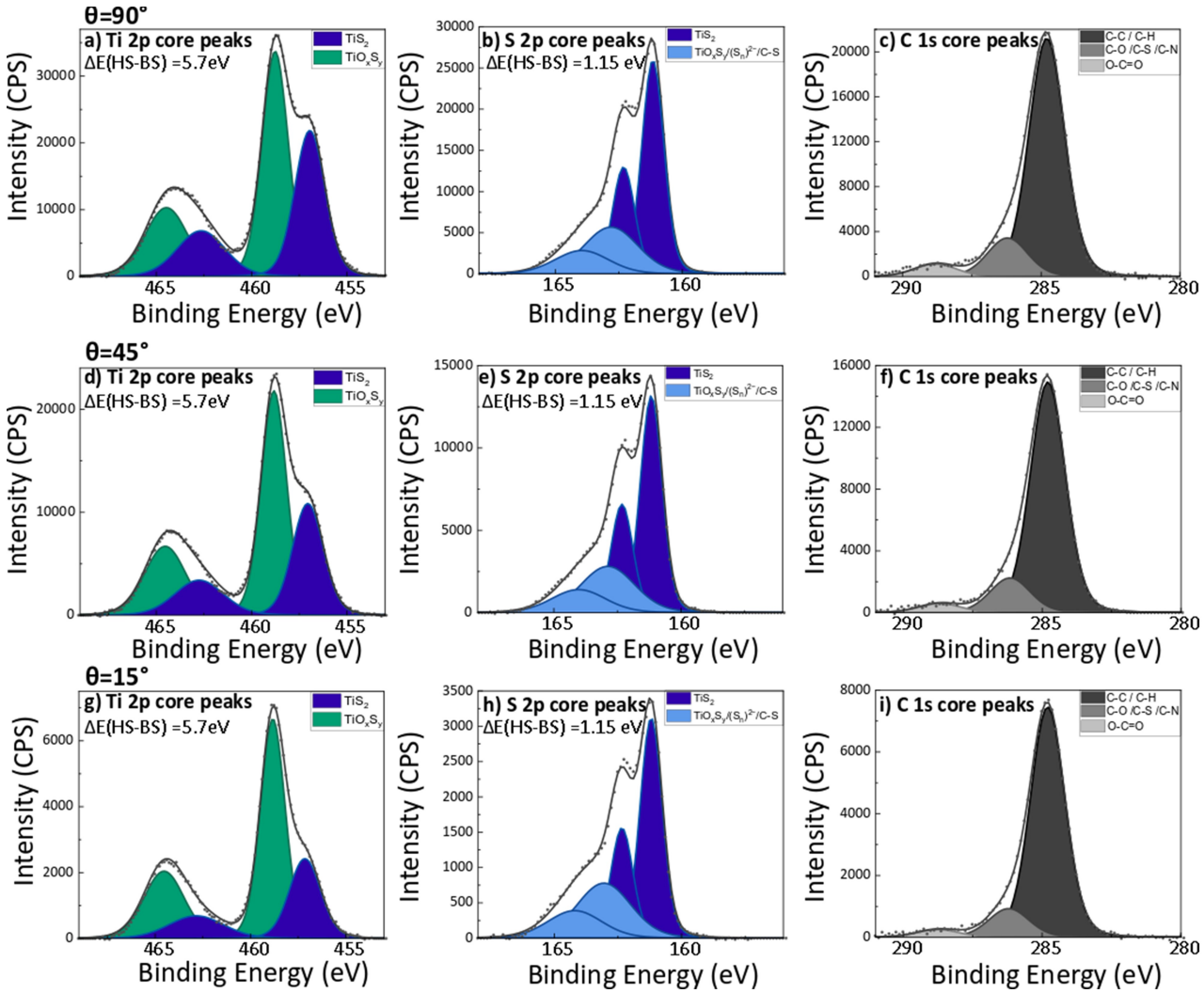

FIG. 4. XPS spectra of Ti 2p, S 2p and C 1s core measured at different angles (θ= 90° (a-c), 45° (d-f) and 15° (g-i)) with respect to the surface normal for the annealed 60-cycle ALD/MLD Ti-thiolate sample using annealing strategy A.

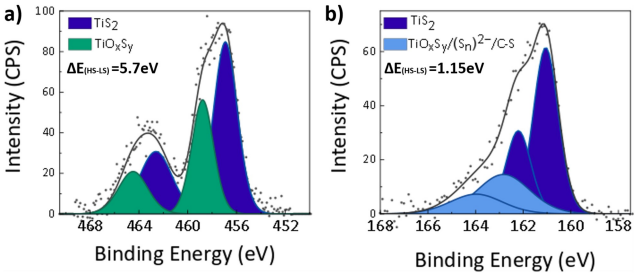

FIG. 5. HAXPES spectra measured with the Cr Kα source for the annealed 60-cycle ALD/MLD Ti-thiolate using annealing strategy A: Intensity as a function of the electron binding energy a) Ti-2p core peaks (doublets) and (b) S-2p core peaks (doublets).

stoichiometric TiS_2.

The atomic ratio [S]/[Ti] using the Cr source (equal to 2.3, see Deep blue column in Figure 6), is in agreement with the Al source (equal to 1.9, see Red column in Figure 6). The difference in values can be explained by the large sampling depth variation between the two sources (minimizing the contribution of the upper surface of the sample using the Cr source and decreasing the uncertainty on the Ti2p spectra fitting). To compare *in situ* XRF and HAXPES results, the total amount of S over the total amount of Ti, determined by HAXPES, was calculated (Light blue column in Figure 6), since XRF cannot identify the elemental composition and attribution of each element. Additional quantitative details are presented (see supplementary material at [URL will be inserted by AIP Publishing] for Table S2). In Figure 6, both the HAXPES (blue columns) and in situ XRF (Yellow column) [S]/[Ti] ratio are almost the same confirming the calibration method of the XRF [S]/[Ti] ratio by the ratio calculated by XPS/HAXPES with a thicker stoichiometric crystalline TiS_2 reference film.

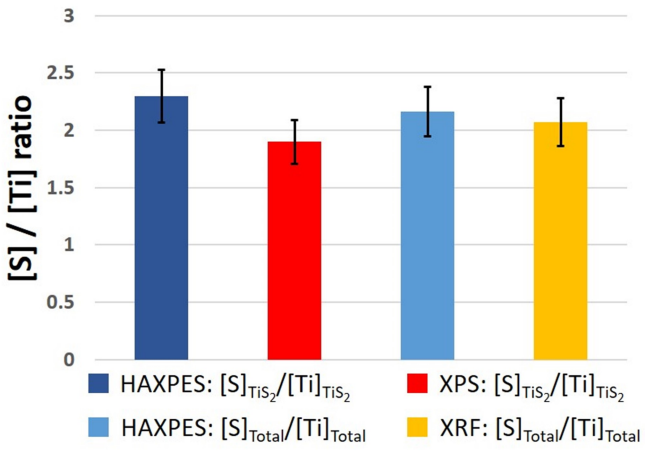

FIG. 6. Stoichiometry study and correlation of results obtained by HAXPES, XPS and *in situ* XRF for 60-cycle ALD/MLD Ti-thiolate annealed under $Ar/H_2(5\%)$ using the annealing strategy A. Black brackets present the measurement error bars.

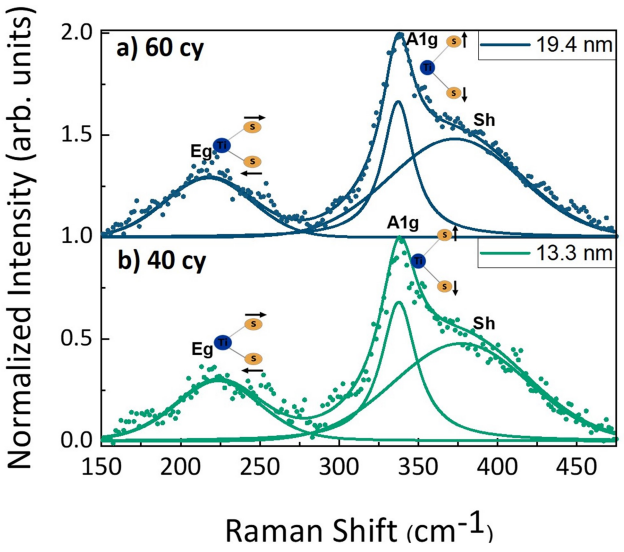

FIG. 7. Raman spectra (dots) of samples resulting from a) 60-cycle and b) 40-cycle ALD/MLD Ti-thiolates after annealing under $Ar/H_2(5\%)$ using annealing strategy A. Raman spectra were normalized to the intensity of the A1g mode. Lorentzian function was used to fit the A1g mode and Gaussian-Lorentzian function to fit the Eg and Sh modes (solid lines in a) and b) panels).

c. Microstructural-crystallinity analysis of the 60-cycle and 40-cycle ALD/MLD annealed samples: Raman scattering spectroscopy and Electron microscopy

Since the thermal annealing strategy A succeeded to give quasi-stoichiometric TiS_2 layers from a 60-cycle ALD/MLD thiolate, the capacity of obtaining ultra-thin TiS_2 thin films using this strategy was explored. Hence, 40-cycle ALD/MLD thiolate were grown and annealed with strategy A.

After annealing, the thickness of the 60-cycle and 40-cycle ALD/MLD films determined by the fitting of XRR curves, were 19.4±0.4 nm and 13.3±0.2 nm, respectively (see supplementary material at [URL will be inserted by AIP Publishing] for Figure S5-(a,b)). The Raman spectra of these two samples are shown in Figure 7-a,b), respectively. The Eg, A1g and Sh- characteristic modes of 1T-TiS_2[21,40,55,60–64] are observed at around 218.2 cm^{-1}, 336.8 cm^{-1} and 375.0 cm^{-1}, for the 60-cycle, and at around 224.3 cm^{-1}, 337.6 cm^{-1} and 378.0 cm^{-1} for the 40-cycle sample one. The observed Raman shift in the position of the Eg mode is assigned to the thickness variation of the thin film.[21] By comparison with the results found in the literature and obtained with a reference TiS_2 powder, the overall spectra indicate the good crystalline quality of the samples with likely some defaults in between the layers as corroborated by the presence of the Sh mode.[21,27]

TEM images (Figure 8-a) reveal a continuous thin film, with low surface roughness. The nanoscale structure shows the presence of textured nanodomains made of a few TiS_2 layers, in agreement with the Raman data discussed above. The interlayer distance between TiS_2 layers is equal to 5.8±0.1 Å close to the bulk 1T-TiS_2 c-parameter, 5.7 Å (PDF 01-070-6204, and[65]). The lamellar sulfide is covered by an amorphous 2 nm-thick top layer, which presumably results from the hydrolysis and oxidation of the material exposed to air, and should therefore probably be titanium oxysulfide. This could be corroborated with the ARXPS results related to surface oxide thickness estimation. At the bottom, the sulfide film/SiO_2 interface is not sharper. The interface regions, about 2 nm thick, are likely to be oxysulfides resulting from chemical reaction with oxygen from the air on one hand; and precursors with the silicon oxide substrate surface on the other.

EDX element mapping in Figure 8 b-e shows the distribution of the elements inside the thin film. The oxidized layer is evidenced by the difference in thickness of the Ti and S maps (Figure 8 b and c, respectively) and the O mapping (Figure 8 d). C elemental mapping (Figure 8 e) suggests an important carbon content inside the thin film, which is in agreement with HAXPES analysis (about 25% of carbon content). In addition, to protect the thin film integrity during TEM preparation a Carbon film was deposited on top of the sample. Concerning the stoichiometry, HAXPES study of the annealed 40-cycle ALD/MLD sample still shows an atomic ratio [S]/[Ti] close to 2.3 in agreement with the value obtained for the 60-cycle one the elemental chemical component and attribution are listed (see supplementary material at [URL will be inserted by AIP Publishing] for Table S3). All those confirm the global stoichiometry of the obtained TiS_2 layers, even for a film as thin as 13.3 nm.

2. *Thermal annealing strategy B*

a. Strategy description

While annealing strategy A has allowed to synthesize thin films composed of good quality TiS_2 layered domain, the deposit is however composed of a significant quantity of carbon and of bridging sulfur which probably hinder a large scale crystallization and explain the presence of amorphous areas in the film (observed in TEM). Several questions are pending:

- At which temperature does the transition from amor-

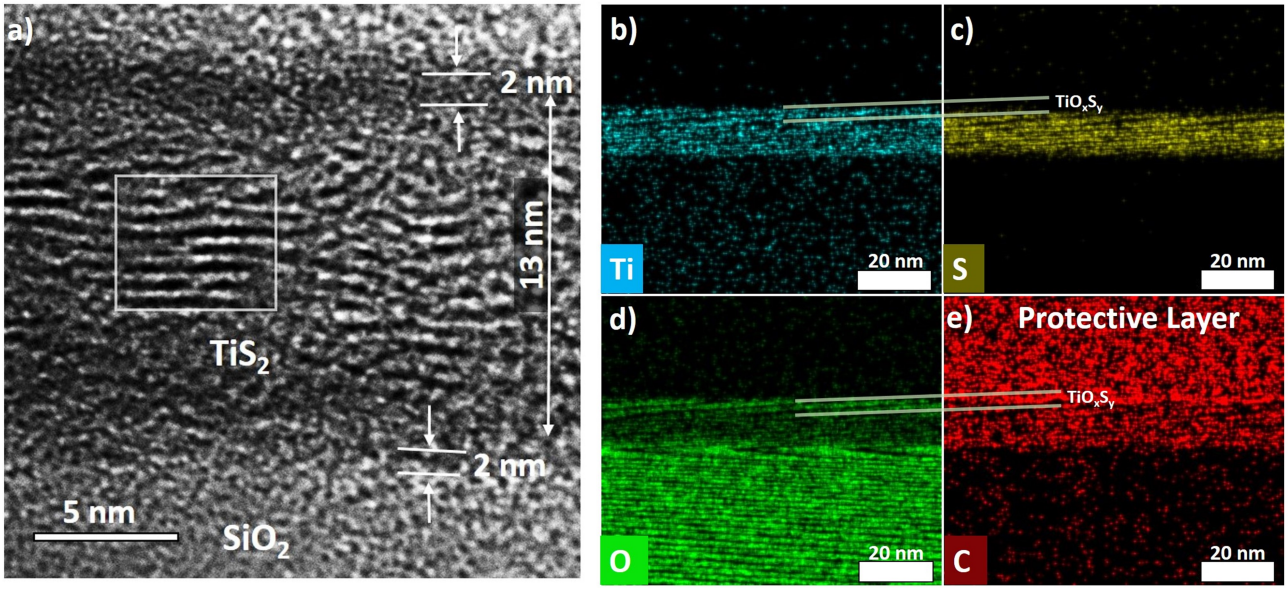

FIG. 8. a) Cross section TEM images and b-e) element mappings (EDX) of b) Ti, c) S, d) O and e) C elements of a sample obtained from 40 ALD/MLD cycles and annealed under Ar/H_2(5%) using the annealing strategy A.

phous to crystalline occur?

- Does the time of annealing play an important role in terms of enhancing the quality of the annealed film?
- Strategy A has allowed to obtain good quality of TiS_2 at 385 °C, compared to 450 °C in the previous study.[40] Is it necessary to anneal at temperature as high as 385 °C ?, or is it possible obtain TiS_2 by annealing at even lower temperature?

To answer these questions, a second annealing strategy, referred to **annealing strategy B**, was applied.

In section III B 1, the fast decrease of the [S]/[Ti] ratio in the temperature range of 50 °C-315 °C confirms that the loss of organic moieties occurs below 300°C and a fully inorganic sample is reached by 300°C (Figure 3). For this reason, the annealing temperature was kept at 300 °C, and the evolution of the [S]/[Ti] ratio determined by *in situ* XRF (Figure 9).

Annealing strategy B was applied on a Ti-thiolate thin film obtained from 40 ALD/MLD cycles. Its thickness, determined by fitting an XRR curve measured *in situ* before annealing, was equal to 32±3 nm. The [S]/[Ti] ratio rapidly decreased while the annealing temperature reached 300 °C at the rate of 10 °C/min. After 135 min at 300 °C, the [S]/[Ti] ratio stabilized near the value of 2. Then the sample was cooled down to room temperature. After annealing, the sample thickness as determined by XRR was equal to 13.9±0.3nm (see supplementary material at [URL will be inserted by AIP Publishing] for Figure S5-c) and the XRF [S]/[Ti] ratio was about 2.

b. Toward ultra-thin thin films: A major challenge

The same strategy (B) was applied to anneal a 20-cycle ALD/MLD Ti-thiolate aiming to lower even further the number of TiS_2 layers. After annealing, the thickness of the sample as determined by XRR was 5.5±0.4 nm (see supplementary material at [URL will be inserted by AIP Publishing] for Figure S5-d). Then, the efficiency of the annealing was further evaluated by elemental and structural characterizations of the thin film. Raman spectra were performed on both annealed 40- and 20-cycle ALD/MLD thiolates to evaluate their crystallinity (Figure 10-a&-b, respectively). It shows the presence of Eg, A1g and Sh- characteristic modes of 1T-TiS_2 at

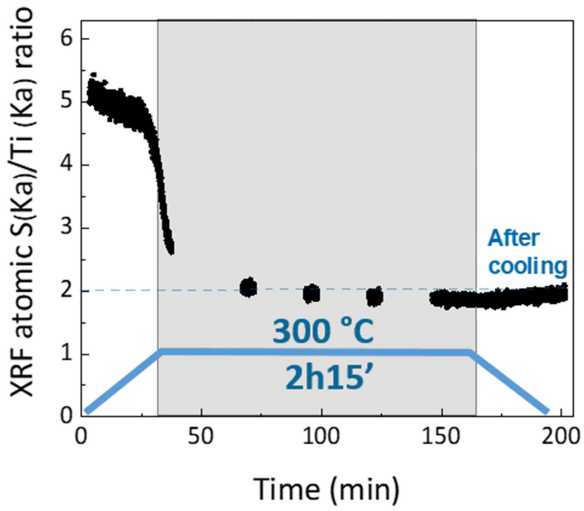

FIG. 9. Calibrated XRF [S]/[Ti] atomic ratio as a function of time and substrate temperature during the annealing under Ar/H_2(5%) of a 40-cycle ALD/MLD Ti-thiolate. This annealing is referred as strategy B.

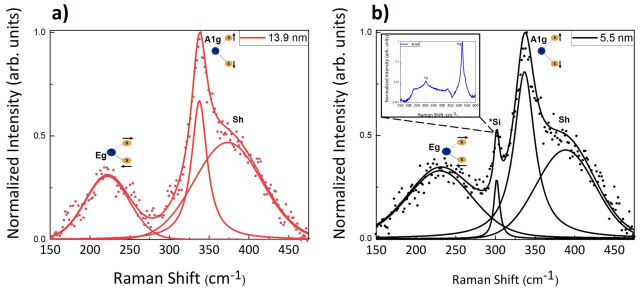

FIG. 10. Raman spectra (dots) of a) 40-cycle and b) 20-cycle ALD/MLD Ti-thiolates annealed under Ar/H_2(5%) using annealing strategy B. Raman spectra were normalized to the intensity of the A1g mode and fitted with Lorentzian function (A1g and *Si modes) and Gaussian-Lorentzian function (Eg and Sh modes) (solid lines panels). The inset in b) show Raman spectrum of Silicon substrate.

222.7 cm^{-1}, 337.7 cm^{-1} and 376.0 cm^{-1}, for 40-cycle, and at around 234.0 cm^{-1}, 336.7 cm^{-1}, and 390.0 cm^{-1} for 20-cycle one. In case of 20-cycle, the spectrum shows the contribution of the silicon-substrate at $\sim$ 300 cm^{-1} (corresponding to the 2nd order mode of silicon) (see inset in Figure 10-b).

The presence of the signal of the underlaying substrate attests that the penetration depth of the excitation laser (532 nm) is higher than the thickness of the thin film. In other words, this confirms the ultra-thin thickness of the annealed 20-cycle ALD/MLD sample.

TEM image of the annealed 20-cycle ALD/MLD sample annealed is shown in Figure 11-a, reveals a continuous thin film with low surface roughness. TiS_2 layers are not visible, which seems contradictory to Raman observations. This could be due to the presence of oxygen or electron beam damage, since the sample is only few nanometers thick (5.5 nm).

Elemental distribution inside the ultra-thin film was provided by EDX mapping as shown in Figure 11 b-e. The Ti and S mappings (Figure 11 b and c, respectively) show a Ti containing thin film with an upper S depleted region. The latter, was also confirmed by the O mapping in Figure 11-d, demonstrating the presence of an oxidized region. The evidence of an upper oxide thin film is in agreement with the EDX observations performed on the 40-cycle ALD/MLD sample annealed with strategy A (see Figure 8-b-c).

HAXPES measurements were performed on both films to check their chemical composition. Binding energies (BE) and atomic concentrations (at.%) of the different chemical environments identified by HAXPES are reported (see supplementary material at [URL will be inserted by AIP Publishing] for Table S4 and Table S5). As reported above, the atomic ratio [S]/[Ti] considering the Ti2p and S2p doublets attributed to TiS_2 were calculated and found equal to 2.3 for both samples, confirming the synthesis of quasi-stoichiometric TiS_2. Although the annealed 20-cycle ALD/MLD sample is very thin, (less than 6 nm thick), a significant carbon content is still detected (around 15% according to HAXPES). Finally, the thickness of the oxidized layer on the top of TiS_2 is almost the same (about 2 nm), no matter what annealing strategy was

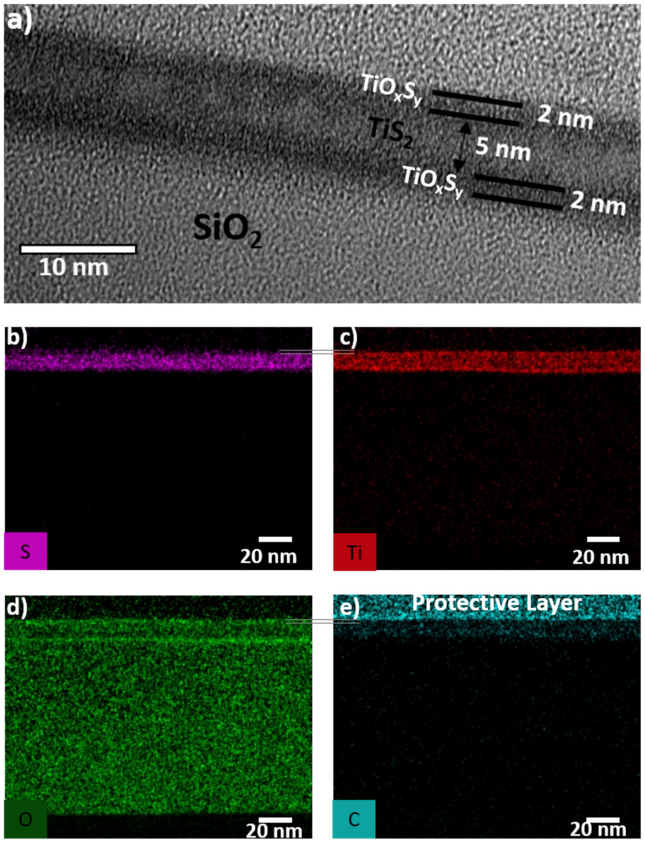

FIG. 11. a) Cross section TEM images and element mapping (EDX) of b) S, c) Ti, d) O and e) C elements of a 20-cycle ALD/MLD sample annealed under Ar/H_2(5%) using thermal annealing strategy B.

applied (also in agreement with our previous work[40]).

To obtain additional information about the local structure of the annealed samples, as a function of annealing treatment and film thickness, we measured XANES spectra at the S K-edge (2742 eV) with the X-ray beam polarization vector parallel to the sample surface. Some of them are represented in Figure 12.

Note that the contribution to the XANES spectra of the oxidized regions, which are present at the sample surface and sulfide/SiO_2 interface, must be small at the sulfur K-edge, because sulfur atoms were mostly removed out of these ill-ordered regions (see Figure 8a, 11b). On contrary, the XANES spectra recorded at the Ti K-edge are sensitive to these regions, the thinner the film the more these regions contribute to the XANES spectra.

In a previous XANES study at the Ti K-edge, we demonstrated that the XANES spectra of the 40-cycle and 80-cycle ALD/MLD samples annealed at 450 °C for 30 min, showed close similarities (features) with the reference XANES spectrum of a TiS_2 powder.[40] The same behavior is observed at the S K-edge (see (b), (c) and (d) spectra in Figure 12).

Figure 12 (a) and (e) show the XANES spectra measured at the S K-edge of a 20-cycle ALD/MLD Ti-thiolate after two different annealing: at 450 °C for 30 min (Ar/H_2(4%)

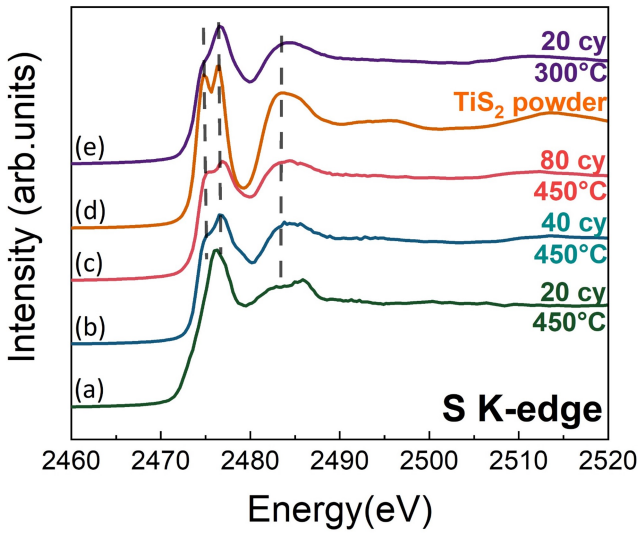

FIG. 12. XANES spectra recorded at the S K-edge of Ti-thiolate thin films further annealed under Ar/H_2(4%) gas at 450 °C for 30 minutes, obtained from (a) 20-cycle ALD/MLD, (b) 40-cycle ALD/MLD and (c) 80-cycle ALD/MLD; (d) XANES spectrum of a reference TiS_2 powder recorded in fluorescence mode; (e) XANES spectrum of a 20-cycle ALD/MLD thin film annealed under Ar/H_2(5%) gas using thermal annealing strategy B.

gas, temperature ramp 10°C/min), and using thermal annealing strategy B (Ar/H_2(5%) gas, temperature ramp 10°C/min). The thicknesses of the two films were 8 and 5.5 nm, respectively. The XANES spectrum of the sample annealed with strategy B presents close similarities to the spectrum of TiS_2 powder reference, while that of the sample annealed at 450 °C is very different.

These XANES results allows us to conclude that the thermal annealing strategy B led to atomic local order which tends to the one of TiS_2 layers. Also, it confirms that the strategy to adopt for the mineralization of the Ti-thiolate and obtain the desired crystalline phase depends on the target film thickness. The quantitative simulations of these spectra is out the scope of this article and will the subject of another one.

IV. CONCLUSIONS AND PERSPECTIVES

The main challenge of this study was to understand and control the transition from amorphous Ti-thiolate thin films to ultra-thin TiS_2 films. Two different thermal annealing strategies were optimized using *in situ* XRF that allows a monitoring of the [S]/[Ti] ratio during the annealing step.

This work highlighted the importance of the annealing step for the synthesis of ultra-thin layered films. *In situ* X-ray synchrotron measurements performed during the annealing and *ex situ* characterizations carried out by XPS, HAXPES, TEM, XANES, and Raman scattering confirmed that appropriate annealing conditions allow to reach an ultra-thin TiS_2 film of thickness down to 5.5 nm. However, the formation of a thin oxide on top of the TiS_2 film at air ambient (which was found to be a constant coverage layer regardless of the annealing strategy) was also evidenced. In the future, an appropriate method to etch the top oxide layer without affecting the quality of the TiS_2 thin film or to protect it from oxidation will be required.

This hybrid ALD/MLD process seems very well adapted to explore other TMDs and opens new possibilities for the synthesis of 2D materials in general. Additionally, the successful growth of an ultra-thin stoichiometric crystalline TiS_2 over an amorphous SiO_2 layer at mild temperature (300 °C) could presents a major advantage toward the integration of such process for back-end-of-line (BEOL) technologies in microelectronics.[66]

ACKNOWLEDGMENTS

The work was financially supported by the ANR project ANR-18-CE09-0031. The Ph.D. work of P.A.Y. is financed by the Labex MINOS (ANR-10-LABX-55-01). The authors acknowledge the facilities and the scientific and technical assistance of the CMTC characterization platform of Grenoble INP supported by the Centre of Excellence of Multifunctional Architectured Materials (CEMAM) ANR-10-LABX-44-01 funded by the "Investments for the Future" Program; as well as facilities at the IRCELYON (UMR 5256 under double tutelage CNRS and Université Claude Bernard Lyon 1) and CP2M laboratories (UMR 5128, under triple tutelage CNRS, CPE Lyon, and Université Claude Bernard Lyon 1, into which the former unit C2P2 UMR 5265 where part of this work was carried out merged). The experiment at the SIRIUS beamline benefited from the SOLEIL beam time allocation no. 20200683. SIRIUS HV diffractometer was funded by the Swedish Research Council (Vetenskapsrådet MAX IV–SOLEIL collaboration) and by the Île-de-France region (project 'FORTE', DIM OXYMORE). A part of this work, carried out on the Platform for Nanocharacterisation (PFNC), was supported by the "Recherche Technologique de Base" program of the French National Research Agency (ANR). We also acknowledge the support of the Tandems collaboration project between PHI and Leti. We acknowledge D. De Barros for ALD reactor engineering assistance and SERMA technologies for TEM measurements.

AUTHOR DECLARATION

Conflict of interest

The authors have no conflicts to disclose.

DATA AVAILABILITY STATEMENT

The data that support the findings of this study are available from the corresponding author upon reasonable request.

REFERENCES

[1] F. N. Sayed, M. Sreedhara, A. Soni, U. Bhat, R. Datta, A. J. Bhattacharyya, and C. Rao, "Li and na-ion diffusion and intercalation characteristics in vertically aligned tis2 nanowall network grown using atomic layer deposition," Materials Research Express **6**, 115549 (2019).

[2] F. Flamary-Mespoulie, A. Boulineau, H. Martinez, M. R. Suchomel, C. Delmas, B. Pecquenard, and F. Le Cras, "Lithium-rich layered titanium sulfides: Cobalt-and nickel-free high capacity cathode materials for lithium-ion batteries," Energy Storage Materials **26**, 213–222 (2020).

[3] L. Zhang, D. Sun, J. Kang, H.-T. Wang, S.-H. Hsieh, W.-F. Pong, H. A. Bechtel, J. Feng, L.-W. Wang, E. J. Cairns, *et al.*, "Tracking the chemical and structural evolution of the tis2 electrode in the lithium-ion cell using operando x-ray absorption spectroscopy," Nano letters **18**, 4506–4515 (2018).

[4] G. A. Muller, J. B. Cook, H.-S. Kim, S. H. Tolbert, and B. Dunn, "High performance pseudocapacitor based on 2d layered metal chalcogenide nanocrystals," Nano letters **15**, 1911–1917 (2015).

[5] V. Pore, M. Ritala, and M. Leskelä, "Atomic layer deposition of titanium disulfide thin films," Chemical Vapor Deposition **13**, 163–168 (2007).

[6] D. Harshman and A. Mills Jr, "Concerning the nature of high-t c superconductivity: Survey of experimental properties and implications for interlayer coupling," Physical Review B **45**, 10684 (1992).

[7] C. Wan, Y. Kodama, M. Kondo, R. Sasai, X. Qian, X. Gu, K. Koga, K. Yabuki, R. Yang, and K. Koumoto, "Dielectric mismatch mediates carrier mobility in organic-intercalated layered tis2," Nano letters **15**, 6302–6308 (2015).

[8] Y. Ye, Y. Wang, Y. Shen, Y. Wang, L. Pan, R. Tu, C. Lu, R. Huang, and K. Koumoto, "Enhanced thermoelectric performance of xmos2–tis2 nanocomposites," Journal of Alloys and Compounds **666**, 346–351 (2016).

[9] M. Barawi, E. Flores, M. Ponthieu, J. R. Ares, F. Cuevas, F. Leardini, I. Ferrer, and C. Sánchez, "Hydrogen storage by titanium based sulfides: nanoribbons (tis3) and nanoplates (tis2)," J. Electr. Eng **3**, 24–29 (2015).

[10] J. H. Han, S. Lee, D. Yoo, J.-H. Lee, S. Jeong, J.-G. Kim, and J. Cheon, "Unveiling chemical reactivity and structural transformation of two-dimensional layered nanocrystals," Journal of the American Chemical Society **135**, 3736–3739 (2013).

[11] E. A. Suslov, O. V. Bushkova, E. A. Sherstobitova, O. G. Reznitskikh, and A. N. Titov, "Lithium intercalation into tis2 cathode material: phase equilibria in a li–tis2 system," Ionics **22**, 503–514 (2016).

[12] X. C. Wu, Y. R. Tao, and Q. X. Gao, "Preparation and field emission properties of titanium polysulfide nanobelt films," Nano Research **2**, 558–564 (2009).

[13] V. Brune, M. Grosch, R. Weißing, F. Hartl, M. Frank, S. Mishra, and S. Mathur, "Influence of the choice of precursors on the synthesis of two-dimensional transition metal dichalcogenides," Dalton Transactions **50**, 12365–12385 (2021).

[14] S. Hao, X. Zhao, Q. Cheng, Y. Xing, W. Ma, X. Wang, G. Zhao, and X. Xu, "A mini review of the preparation and photocatalytic properties of two-dimensional materials," Frontiers in Chemistry **8**, 582146 (2020).

[15] E. S. Peters, C. J. Carmalt, and I. P. Parkin, "Dual-source chemical vapour deposition of titanium sulfide thin films from tetrakisdimethylamidotitanium and sulfur precursors," Journal of Materials Chemistry **14**, 3474–3477 (2004).

[16] R. G. Palgrave and I. P. Parkin, "Chemical vapour deposition of titanium chalcogenides and pnictides and tungsten oxide thin films," New Journal of Chemistry **30**, 505–514 (2006).

[17] C. J. Carmalt, I. P. Parkin, and E. S. Peters, "Atmospheric pressure chemical vapour deposition of tis2 thin films on glass," Polyhedron **22**, 1263–1269 (2003).

[18] C. J. Carmalt, S. A. O'Neill, I. P. Parkin, and E. S. Peters, "Titanium sulfide thin films from the aerosol-assisted chemical vapour deposition of [ti (sbu t) 4]," Journal of Materials Chemistry **14**, 830–834 (2004).

[19] K. Kanehori, Y. Ito, F. Kirino, K. Miyauchi, and T. Kudo, "Titanium disulfide films fabricated by plasma cvd," Solid State Ionics **18**, 818–822 (1986).

[20] J. Cheon, J. E. Gozum, and G. S. Girolami, "Chemical vapor deposition of mos2 and tis2 films from the metal- organic precursors mo (s-t-bu) 4 and ti (s-t-bu) 4," Chemistry of materials **9**, 1847–1853 (1997).

[21] P. C. Sherrell, K. Sharda, C. Grotta, J. Ranalli, M. S. Sokolikova, F. M. Pesci, P. Palczynski, V. L. Bemmer, and C. Mattevi, "Thickness-dependent characterization of chemically exfoliated tis2 nanosheets," ACS omega **3**, 8655–8662 (2018).

[22] V. V. Plashnitsa, F. Vietmeyer, N. Petchsang, P. Tongying, T. H. Kosel, and M. Kuno, "Synthetic strategy and structural and optical characterization of thin highly crystalline titanium disulfide nanosheets," The journal of physical chemistry letters **3**, 1554–1558 (2012).

[23] N. Mahuli and S. K. Sarkar, "Atomic layer deposition of titanium sulfide and its application in extremely thin absorber solar cells," Journal of Vacuum Science & Technology A: Vacuum, Surfaces, and Films **33**, 01A150 (2015).

[24] H. Nam, H. Yang, E. Kim, C. Bae, and H. Shin, "Semiconducting tio2- xsx thin films by atomic layer deposition of tis2 and its oxidation in ambient," Journal of Vacuum Science & Technology A: Vacuum, Surfaces, and Films **37**, 020916 (2019).

[25] A. Aljabour, H. Coskun, X. Zheng, M. G. Kibria, M. Strobel, S. Hild, M. Kehrer, D. Stifter, E. H. Sargent, and P. Stadler, "Active sulfur sites in semimetallic titanium disulfide enable co2 electroreduction," ACS Catalysis **10**, 66–72 (2019).

[26] X. Zang, C. Shen, E. Kao, R. Warren, R. Zhang, K. S. Teh, J. Zhong, M. Wei, B. Li, Y. Chu, *et al.*, "Titanium disulfide coated carbon nanotube hybrid electrodes enable high energy density symmetric pseudocapacitors," Advanced materials **30**, 1704754 (2018).

[27] S. B. Basuvalingam, Y. Zhang, M. A. Bloodgood, R. H. Godiksen, A. G. Curto, J. P. Hofmann, M. A. Verheijen, W. M. Kessels, and A. A. Bol, "Low-temperature phase-controlled synthesis of titanium di-and tri-sulfide by atomic layer deposition," Chemistry of Materials **31**, 9354–9362 (2019).

[28] M. Mattinen, F. Gity, E. Coleman, J. F. Vonk, M. A. Verheijen, R. Duffy, W. M. Kessels, and A. A. Bol, "Atomic layer deposition of large-area polycrystalline transition metal dichalcogenides from 100° c through control of plasma chemistry," Chemistry of Materials **34**, 7280–7292 (2022).

[29] J. G. van Kasteren, S. B. Basuvalingam, M. Mattinen, A. E. Bracesco, W. M. Kessels, A. A. Bol, and B. Macco, "Growth mechanism and film properties of atomic-layer-deposited titanium oxysulfide," Chemistry of Materials **34**, 7750–7760 (2022).

[30] S. M. George, "Atomic layer deposition: an overview," Chemical reviews **110**, 111–131 (2010).

[31] B. Chatmaneerungcharoen, M. Fraccaroli, F. Martin, C. Guedj, E. Nolot, D. Rouchon, N. Vaxelaire, R. Templier, A. Grenier, A.-M. Papon, *et al.*, "Synthesis of in-plane oriented tin sulfides by organosulfur-mediated sulfurization of ultrathin sno2 films," Chemistry of Materials **34**, 5842–5851 (2022).

[32] H. Zhang, T. van Pelt, A. N. Mehta, H. Bender, I. Radu, M. Caymax, W. Vandervorst, and A. Delabie, "Nucleation and growth mechanism of 2d sns2 by chemical vapor deposition: Initial 3d growth followed by 2d lateral growth," 2D Materials **5**, 035006 (2018).

[33] G.-H. Park, K. Nielsch, and A. Thomas, "2d transition metal dichalcogenide thin films obtained by chemical gas phase deposition techniques," Advanced Materials Interfaces **6**, 1800688 (2019).

[34] J. Cai, X. Han, X. Wang, and X. Meng, "Atomic layer deposition of two-dimensional layered materials: processes, growth mechanisms, and characteristics," Matter **2**, 587–630 (2020).

[35] M. Mattinen, M. Leskelä, and M. Ritala, "Atomic layer deposition of 2d metal dichalcogenides for electronics, catalysis, energy storage, and beyond," Advanced Materials Interfaces **8**, 2001677 (2021).

[36] Y. Kim, W. J. Woo, D. Kim, S. Lee, S.-m. Chung, J. Park, and H. Kim, "Atomic-layer-deposition-based 2d transition metal chalcogenides: Synthesis, modulation, and applications," Advanced Materials **33**, 2005907 (2021).

[37] J. Multia and M. Karppinen, "Atomic/molecular layer deposition for designer's functional metal–organic materials," Advanced Materials Interfaces **9**, 2200210 (2022).

[38] P. Sundberg and M. Karppinen, "Organic and inorganic–organic thin film structures by molecular layer deposition: A review," Beilstein journal of nanotechnology **5**, 1104–1136 (2014).

[39] Y. Zhao, L. Zhang, J. Liu, K. Adair, F. Zhao, Y. Sun, T. Wu, X. Bi, K. Amine, J. Lu, *et al.*, "Atomic/molecular layer deposition for energy storage and conversion," Chemical Society Reviews **50**, 3889–3956 (2021).

[40]P. Abi Younes, E. Skopin, M. Zhukush, L. Rapenne, H. Roussel, N. Aubert, L. Khrouz, C. Licitra, C. Camp, M.-I. Richard, *et al.*, "Transition metal dichalcogenide tis2 prepared by hybrid atomic layer deposition/molecular layer deposition: Atomic-level insights with in situ synchrotron x-ray studies and molecular surface chemistry," Chemistry of Materials (2022).

[41]G. Ciatto, M. Chu, P. Fontaine, N. Aubert, H. Renevier, and J. Deschanvres, "Sirius: A new beamline for in situ x-ray diffraction and spectroscopy studies of advanced materials and nanostructures at the soleil synchrotron," Thin Solid Films **617**, 48–54 (2016).

[42]R. Boichot, L. Tian, M.-I. Richard, A. Crisci, A. Chaker, V. Cantelli, S. Coindeau, S. Lay, T. Ouled, C. Guichet, *et al.*, "Evolution of crystal structure during the initial stages of zno atomic layer deposition," Chemistry of Materials **28**, 592–600 (2016).

[43]H. Shinotsuka, S. Tanuma, and C. J. Powell, "Calculations of electron inelastic mean free paths. xiii. data for 14 organic compounds and water over the 50 ev to 200 kev range with the relativistic full penn algorithm," Surface and Interface Analysis **54**, 534–560 (2022).

[44]D. Verner, G. J. Ferland, K. Korista, and D. Yakovlev, "Atomic data for astrophysics. ii. new analytic fits for photoionization cross sections of atoms and ions," arXiv preprint astro-ph/9601009 (1996).

[45]G. Ciatto, N. Aubert, M. Lecroard, C. Engblom, P. Fontaine, J.-M. Dubuisson, Y.-M. Abiven, P.-E. Janolin, J.-M. Kiat, Y. Dumont, *et al.*, "Forte–a multipurpose high-vacuum diffractometer for tender x-ray diffraction and spectroscopy at the sirius beamline of synchrotron soleil," Journal of Synchrotron Radiation **26**, 1374–1387 (2019).

[46]J. L. Brito, M. Ilija, and P. Hernández, "Thermal and reductive decomposition of ammonium thiomolybdates," Thermochimica Acta **256**, 325–338 (1995).

[47]H. Lin, L. Yang, X. Jiang, G. Li, T. Zhang, Q. Yao, G. W. Zheng, and J. Y. Lee, "Electrocatalysis of polysulfide conversion by sulfur-deficient mos_2 nanoflakes for lithium–sulfur batteries," Energy & Environmental Science **10**, 1476–1486 (2017).

[48]Y. Altowairqi, A. Alsubaie, K. Stroh, I. Perez-Marin, L. Bowen, M. Szablewski, and D. Halliday, "The effect of annealing conditions: temperature, time, ramping rate and atmosphere on nanocrystal Cu2ZnSnS4 (CZTS) thin film solar cell properties," Materials Today: Proceedings **18**, 473–486 (2019).

[49]S. Cadot, O. Renault, M. Frégnaux, D. Rouchon, E. Nolot, K. Szeto, C. Thieuleux, L. Veyre, H. Okuno, F. Martin, *et al.*, "A novel 2-step ald route to ultra-thin mos 2 films on sio 2 through a surface organometallic intermediate," Nanoscale **9**, 538–546 (2017).

[50]H. Martinez, C. Auriel, D. Gonbeau, M. Loudet, and G. Pfister-Guillouzo, "Studies of 1t tis2 by stm, afm and xps: the mechanism of hydrolysis in air," Applied surface science **93**, 231–235 (1996).

[51]V. Dubois, B. Pecquenard, S. Soulé, H. Martinez, and F. Le Cras, "Dual cation-and anion-based redox process in lithium titanium oxysulfide thin film cathodes for all-solid-state lithium-ion batteries," ACS Applied Materials & Interfaces **9**, 2275–2284 (2017).

[52]M.-H. Lindic, B. Pecquenard, P. Vinatier, A. Levasseur, H. Martinez, D. Gonbeau, P.-E. Petit, and G. Ouvrard, "Characterization of rf sputtered tioysz thin films," Thin Solid Films **484**, 113–123 (2005).

[53]M.-H. Lindic, H. Martinez, A. Benayad, B. Pecquenard, P. Vinatier, A. Levasseur, and D. Gonbeau, "Xps investigations of tioysz amorphous thin films used as positive electrode in lithium microbatteries," Solid State Ionics **176**, 1529–1537 (2005).

[54]J.-C. Dupin, D. Gonbeau, I. Martin-Litas, P. Vinatier, and A. Levasseur, "Amorphous oxysulfide thin films moysz (m= w, mo, ti) xps characterization: structural and electronic pecularities," Applied surface science **173**, 140–150 (2001).

[55]C. Lin, X. Zhu, J. Feng, C. Wu, S. Hu, J. Peng, Y. Guo, L. Peng, J. Zhao, J. Huang, *et al.*, "Hydrogen-incorporated tis2 ultrathin nanosheets with ultrahigh conductivity for stamp-transferrable electrodes," Journal of the American Chemical Society **135**, 5144–5151 (2013).

[56]M. Seah, J. Qiu, P. Cumpson, and J. Castle, "Simple method of depth profiling (stratifying) contamination layers, illustrated by studies on stainless steel," Surface and interface analysis **21**, 336–341 (1994).

[57]J. Richard, A. Benayad, J.-F. Colin, and S. Martinet, "Charge transfer mechanism into the chevrel phase mo6s8 during mg intercalation," The Journal of Physical Chemistry C **121**, 17096–17103 (2017).

[58]H. Martinez, A. Benayad, D. Gonbeau, P. Vinatier, B. Pecquenard, and A. Levasseur, "Influence of the cation nature of high sulfur content oxysulfide thin films moysz (m= w, ti) studied by xps," Applied surface science **236**, 377–386 (2004).

[59]D. Gonbeau, C. Guimon, G. Pfister-Guillouzo, A. Levasseur, G. Meunier, and R. Dormoy, "Xps study of thin films of titanium oxysulfides," Surface Science **254**, 81–89 (1991).

[60]A. Dużyńska, J. Judek, K. Wilczyński, K. Zberecki, A. Łapińska, A. Wróblewska, and M. Zdrojek, "Temperature-induced phonon behavior in titanium disulfide (tis2) nanosheets," Journal of Raman Spectroscopy **50**, 1114–1119 (2019).

[61]M. Hangyo, S. Nakashima, Y. Hamada, T. Nishio, and Y. Ohno, "Raman scattering from the misfit-layer compounds snnbs 3, pbnbs 3, and pbtis 3," Physical Review B **48**, 11291 (1993).

[62]M. Ishii, M. Saeki, and I. Kawada, "Raman study of non-stoichiometric titanium sulfides," physica status solidi (b) **124**, K109–K112 (1984).

[63]A. L. Let, D. E. Mainwaring, C. J. Rix, and P. Murugaraj, "Thio sol–gel synthesis of titanium disulfide thin films and nanoparticles using titanium (iv) alkoxide precursors," Journal of Physics and Chemistry of Solids **68**, 1428–1435 (2007).

[64]A. L. Let, D. E. Mainwaring, C. Rix, and P. Murugaraj, "Thio sol–gel synthesis of titanium disulfide thin films and powders using titanium alkoxide precursors," Journal of non-crystalline solids **354**, 1801–1807 (2008).

[65]H. Kasai, K. Tolborg, M. Sist, J. Zhang, V. R. Hathwar, M. Ø. Filsø, S. Cenedese, K. Sugimoto, J. Overgaard, E. Nishibori, *et al.*, "X-ray electron density investigation of chemical bonding in van der waals materials," Nature materials **17**, 249–252 (2018).

[66]J. Lin, S. Monaghan, N. Sakhuja, F. Gity, R. K. Jha, E. M. Coleman, J. Connolly, C. P. Cullen, L. A. Walsh, T. Mannarino, *et al.*, "Large-area growth of mos2 at temperatures compatible with integrating back-end-of-line functionality," 2D Materials **8**, 025008 (2020).